

Helium absorption and emission towards Θ^1 Ori C

René D. Oudmaijer,¹ Janet E. Drew,¹ M. J. Barlow,² I. A. Crawford² and D. Proga¹

¹Imperial College of Science, Technology and Medicine, Blackett Laboratory, Prince Consort Road, London SW7 2BZ

²Department of Physics & Astronomy, University College London, Gower Street, London WC1E 6BT

Accepted 1997 June 2. Received 1997 May 28; in original form 1997 March 6

ABSTRACT

The He I absorption and emission systems towards Θ^1 Ori C, the exciting star of the Orion Nebula, are investigated. To this end, high-resolution near-infrared long-slit spectra centred on the He I 1.083- μ m and Br γ lines and an ultra-high-resolution ($R \sim 10^6$) spectrum of the optical He I 3889- \AA line have been obtained. These data are supplemented by blue high spectral resolution echelle observations of Θ^1 Ori C and the other members of the Trapezium. Even at $R \sim 10^6$, the He I absorption profile, associated with foreground gas at a heliocentric velocity of +3 km s $^{-1}$, is very smooth, suggesting a simple broadening mechanism and homogeneity. The combination of the He I 2 3 S column density, deduced from the 3889- \AA line, with the non-detection of Br γ emission at the same velocities sets an upper limit on the electron density in this medium of 10^{10} m^{-3} . The He I 1.083- μ m long-slit spectrum shows the familiar background nebular emission, while a second blueshifted component is visible off-star at the same velocities as the absorption on-star. Several mechanisms to explain this emission are explored. We conclude that it is most probably emission formed behind, and leaking through, the absorbing gas layer. A clue to the origin of this emission is found in its spatial distribution: unlike the bright background nebular emission, the blueshifted component peaks symmetrically around the position of Θ^1 Ori C, suggesting a physical association with the star. A possible model for the blueshifted emission is that it arises in a large-scale, dense shock front, provoked in some way by the wind of Θ^1 Ori C.

Key words: circumstellar matter – stars: early-type – stars: emission-line, Be – stars: individual: Θ^1 Ori C – stars: pre-main-sequence – H II regions.

1 INTRODUCTION

The Orion nebula, M42, at a distance of about 450 pc, is the nearest massive star-forming region, and as such is a key target for the study of the birth of massive stars. Much effort has been spent on modelling the physical conditions and geometry of this nebula. The picture that has emerged is that of a highly obscured region, OMC-1, where star formation is still going on, behind an H II region ionized by the young OB stars of the well-known Trapezium. The brightest member of the Trapezium, Θ^1 Ori C, is also the dominant source of ionizing radiation. Gas in the interface between OMC-1 and the H II region gives rise to the strongest components of nebular emission in M42. Basic physical parameters of this principal ionization front have been determined in studies such as that by Baldwin et al. (1991; see also Baldwin et al. 1996 – and references in both papers).

However, it has long been known that ionized gas can also be traced on the near side of M42 in narrow blueshifted absorption features in the He I 3889- \AA ($2^3S \rightarrow 3^3P^0$) line along the sightlines toward the Trapezium stars (e.g. Adams 1944). The mean velocity of the absorption component common to all of them is measured to

be 2–3 km s $^{-1}$ (heliocentric). This is a blueshift both with respect to Θ^1 Ori C at a radial velocity of 10–15 km s $^{-1}$ (Stahl et al. 1996) and with respect to the main background nebula at $\sim 20 \text{ km s}^{-1}$. The question of the foreground He I absorption has recently been revisited by O'Dell et al. (1993). They conducted a high spectral resolution absorption-line study of these sightlines and proposed that the 2–3 km s $^{-1}$ He I velocity component is produced in a secondary ionization front on the near side (with respect to the observer) of the so-called ‘neutral lid’ – a layer of neutral gas, optically thick in the Lyman continuum, interposed between the nebula and the diffuse interstellar medium (see Savage & Jenkins 1972; van der Werf & Goss 1989). By contrast, Baldwin et al. (1991) preferred to locate this component on the far side of the neutral lid where the ionization would be due to Θ^1 Ori C. No study has gone beyond a tentative explanation of why it is that the sightline towards Θ^1 Ori C uniquely reveals a second, higher velocity, blueshifted He I 3889- \AA feature at $\sim -30 \text{ km s}^{-1}$ in addition to the ubiquitous 2–3 km s $^{-1}$ absorption. The focus in this paper is again on these blueshifted He I triplet-line features. Our contribution is to derive insights from combining data on the 3889- \AA line and long-slit IR echelle observations at He I 1.083 μ m.

Our motivation is the quite common appearance of blueshifted He I absorption in the spectra of the exciting stars of other young, but more heavily obscured, H II regions. For example, Drew, Bunn & Hoare (1993) reported on blueshifted He I 2.058- μm absorption in the spectrum of S106IR; it has since been detected in the Herbig Be star MWC 297 (Murdoch & Drew 1994) and also in the southern BN-type object, IRAS 07173–1733 (Oudmaijer et al., in preparation). One difference is that the absorption associated with these H II regions is substantially broader, indicating relative velocities of $\sim 100 \text{ km s}^{-1}$ or more as compared with just $10\text{--}50 \text{ km s}^{-1}$ for M42. Ultimately, given how much more is known about M42, it should be easier to place the blueshifted He I absorption and associated phenomena into a satisfying dynamical context. In so doing, a clearer picture can be developed of the astrophysics that may also prove relevant to He I line formation in more obscured H II regions where high spectral resolution 3889-Å line observations are infeasible.

Most of our data concern Θ^1 Ori C (HR 1895) and its immediate surroundings. This star is a peculiar, mildly reddened O star (Walborn 1981; see also Walborn & Nichols 1994) powering a dense, high-velocity wind ($\dot{M} = 10^{-6.4} \text{ M}_\odot \text{ yr}^{-1}$, $v_\infty = 1000 \text{ km s}^{-1}$; Howarth & Prinja 1989). We have obtained both high- and ultra-high-resolution echelle spectra at wavelengths spanning the He I 3889-Å line towards Θ^1 Ori C, and high-resolution IR data at the He I 1.083- μm line taken through an east–west long slit crossing the position of Θ^1 Ori C. Both the optical line and the 1.083- μm line arise from the same excited level (2^3S) of neutral helium, a fact that gives considerable leverage in understanding the origin of the latter. A particular concern that emerges in this is the origin of a weak emission component off-star in the 1.083- μm line at similar velocities to the blueshifted 3889-Å absorption. This was first noticed by Vaughan (1968), and further examined by Münch (1986). Neither of these authors was able to account for this phenomenon. We shall show that the options for explaining this emission are in fact very limited.

This paper is organized as follows. In Section 2 we describe the observations. The data derived from them are presented in Sections 3 and 4. In Section 5, the optical and infrared data are used together to set a constraint on the electron density in the foreground absorbing gas. This is then used in determining whether the blueshifted emission may arise in photoionized gas. As this does not seem to be feasible, we then consider and reject the possibility of emission due to scattered starlight. It is proposed, instead, that shock emission leaking through the foreground absorbing layers may be implicated. The paper ends with a short discussion and summary.

2 OBSERVATIONS

2.1 The ultra-high-resolution spectrum

A spectrum of the He I 3889-Å circumstellar absorption line towards Θ^1 Ori C was obtained with the Ultra-High-Resolution Facility (UHRF; Diego et al. 1995) at the 3.9-m Anglo-Australian Telescope on 1994 December 18. A Tektronix 1024 \times 1024 CCD with 24- μm pixels was used as detector and the total integration time was 1500 s. Wavelength calibration was with respect to a Th–Ar arc lamp. The spectral resolution, determined from the FWHM of a frequency-stabilized He–Ne laser observed on the same night, was 0.34 km s^{-1} ($R = 880\,000$). The UHRF was used in its usual image-slicer mode. The signal-to-noise ratio achieved in the local continuum formed by the base of the broad and blended photospheric He I 3889-Å and H8 profiles was 25.

Table 1. Log of the UCLES observations (1995 December 6).

Object	HR number	Spectral type	V	Total exposure (s)	SNR
Θ^1 A Ori	1893	O7	6.73	400	100
Θ^1 B Ori	1894	B0V	7.96	1600	100
Θ^1 C Ori	1895	O6var	5.13	120	160
Θ^1 D Ori	1896	B0.5Vp	6.70	320	150

The signal-to-noise ratio (SNR) is measured around 3890 Å.

The spectral types and V magnitudes are taken from the SIMBAD data base.

2.2 UCLES echelle spectroscopy

During the night of 1995 December 6, Θ^1 Ori C and the other three members of the Trapezium were observed in service time, employing the University College London Echelle Spectrograph (UCLES) mounted on the 3.9-m Anglo-Australian Telescope. The observational set-up included a 0.9-arcsec slit, the 31 groove mm⁻¹ echelle and the same Tektronix CCD detector as used with the UHRF. In the spatial direction, the pixels correspond to 0.3 arcsec. The central wavelength of these observations was 4237 Å, resulting in a spectrum of 33 orders, with a spectral coverage of 3790 to 4875 Å. The observations made of each star were co-added. A log of the observations is provided in Table 1 together with the resulting signal-to-noise ratio in the 3890-Å order.

The data were reduced in the standard way and included the procedures of bias-subtraction, flat-fielding and wavelength calibration. An observation of a Th–Ar arc lamp was used to provide the wavelength calibration of each spectrum. The dispersion fit through more than 400 identified arc lines yielded an rms value of 0.12 km s^{-1} using fourth-order polynomials in both the dispersion and cross-dispersion directions. The resulting spectral resolution was determined to be $\sim 7 \text{ km s}^{-1}$ from Gaussian fits through the arc lines.

2.3 Near-infrared data

Two weeks after the UCLES observations, during the night of 1995 December 22, long-slit spectroscopy of Θ^1 Ori C was carried out with the 3.8-m infrared telescope UKIRT, Hawaii. The CGS4 spectrometer was used, with a cooled 256×256 InSb array as detector. To oversample the resolution element and to allow correction for bad pixels, the array was substepped by a third of a pixel six times over a range of 2 pixel. The slit orientation was in the east–west direction, with a slit width of 1 pixel. The detector pixel sizes were 1.5 arcsec along the slit and 1 arcsec in the dispersion direction (corresponding to $\sim 16 \text{ km s}^{-1}$). Since strong emission is present close to Θ^1 Ori C, sky subtraction was performed using a clear piece of sky, free of nebular emission, that was found approximately 6 arcmin east of Θ^1 Ori C.

Both the He I 1.083- μm and the Brγ 2.166- μm lines were observed in echelle mode. The total on-source integration times were 300 and 360 s respectively. The resulting SNR was about 150 in the stellar continuum around 1.083 μm . In the Brγ spectrum, the achieved SNR is lower than pure Poisson statistics would suggest. This is because the spectrum was affected by fringing at an amplitude of order 5–10 per cent of the continuum that could not be entirely filtered out. Details of the procedure used to remove fringes from CGS4/echelle spectra will appear elsewhere (Oudmaijer et al., in preparation). The removal of the fringes works

satisfactorily in the continuum, but care must be taken when interpreting the profiles of strong emission lines. Each spectrum was corrected for atmospheric absorption and instrumental transmission by dividing it through by a spectrum of a bright comparison star observed at roughly the same airmass. For the He I 1.083- μm setting an A star was used for this purpose, while at Br γ an F or G star was preferred. The Br γ absorption features present in the standard F–G star spectra were removed by fitting to and dividing through by Gaussian profiles.

The wavelength calibration of the He I setting was performed using the xenon arc spectrum. The spectral resolution as determined from the FWHM of the arc lines was 22 km s $^{-1}$. The Br γ calibration was performed using lines of an argon lamp, while the zero-point of the calibration was determined by shifting the spectrum to the rest wavelengths of the strong telluric absorption lines at 2.163 50 and 2.168 77 μm (vacuum).

Flux calibration was performed using the FIGARO task IRFLUX. From the published spectral types and the B and V magnitudes of the standard stars, effective temperatures and predicted J magnitudes were derived using the tables of Straizys & Kurliene (1981) and Koornneef (1983) respectively. IRFLUX then uses the temperature of the standard star to estimate its flux at the observed wavelength. The uncertainty introduced by this procedure, compared with using spectrophotometric standards, is of no significance, because the dominant uncertainty in the continuum flux is due to slit losses.

The resulting continuum flux densities of Θ^1 Ori C using four different standards are consistent with a peak-to-peak variation of only 5 per cent around the mean. We adopt continuum flux values of $F_{1.083} = 7.5 \times 10^{-11} \text{ W m}^{-2} \mu\text{m}^{-1}$ and $F_{2.16} = 7 \times 10^{-12} \text{ W m}^{-2} \mu\text{m}^{-1}$. These values are in good agreement with published broad-band photometry.

The colour excess $E(B - V)$ and the ratio of total to selective reddening, R , towards Θ^1 Ori C were determined by Cardelli, Clayton & Mathis (1989) to be 0.34 and 5.5 respectively. The high value of R indicates a total extinction at the V band of $A_V = 1.87$. Hence the interstellar extinction at 1.083 μm is not negligible. From interpolating the broad-band data of Rieke & Lebofsky (1985) we find that an upward correction of 87 per cent at 1.08 μm and of 21 per cent at K of the observed fluxes is necessary. Calculated using the laws of Cardelli et al. (1989), these corrections would instead be 116 and 26 per cent. Unless specifically stated, we will use the underreddened, observed fluxes.

Finally, all radial velocities cited in this paper are in the heliocentric velocity frame. To convert them to the Local Standard of Rest, 18 km s $^{-1}$ should be subtracted.

3 THE OPTICAL PERSPECTIVE

3.1 He I 3889 Å as observed toward Θ^1 Ori C at ultra-high resolution

Fig. 1 shows the UHRF spectrum of the He I 3889-Å line of Θ^1 Ori C (solid line) with the UCLES spectrum overlaid on it (dotted line). The spectra match well, with the UHRF spectrum just missing the blue wing of the bluer component. The total lack of observable substructure in this ultra-high-resolution spectrum is particularly telling – we can rule out profile substructure on scales at least as fine as 1 km s $^{-1}$.

The FWHM of the blue and red velocity components as measured from the UHRF data are 21 and 14 km s $^{-1}$ respectively. Since the thermal broadening of a spectral line can be expressed as $\text{FWHM} = 21.4 \times \sqrt{t_4/M} \text{ km s}^{-1}$, with t_4 the temperature in 10 4 K,

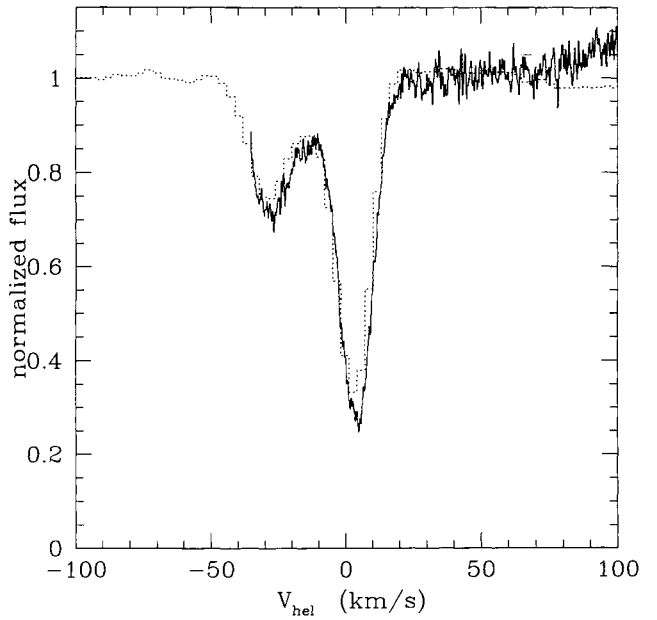


Figure 1. Continuum-normalized spectra around He I 3889 Å obtained with UHRF (solid line) and UCLES (dotted line). The UHRF spectrum has been boxcar-smoothed over 3 pixel. The ‘continuum’ upon which these features are superimposed is the very much broader blend of He I 3889-Å and H8 photospheric lines (e.g. see the lower resolution data shown by Baldwin et al. 1991).

and M the atomic weight, one obtains an expected intrinsic broadening of 10.1 km s $^{-1}$ for a typical electron temperature in the Orion nebula of 9000 K (e.g. Peimbert 1967; Baldwin et al. 1991). In order to reproduce the observed broadening, one needs temperatures of 40 000 and 17 000 K, which are too high to be attributed to photoionization heating only. Alternatively, if the gas temperature is fixed at 9000 K, additional turbulent broadening of 18 and 9.8 km s $^{-1}$ respectively is demanded by the data. Whilst the red component has an implied turbulent velocity comparable with the figure of 8.6 km s $^{-1}$ found in the [O III] lines by Castañeda (1988) for the H II region as a whole, the turbulent width of the blue component clearly is much greater. In any case, an open mind should be retained as to whether this component in particular is fairly represented by a single Gaussian.

3.2 He I 3889 Å as observed toward all Trapezium stars

In Fig. 2, UCLES spectra of the interstellar He I 3889-Å line in the spectra of all Trapezium stars are shown. The component at 3.5 km s $^{-1}$ is present in the spectra of all the stars, suggesting that it may arise in a sheet of gas covering the entire Trapezium system.

In the spectra of Θ^1 Ori B and Θ^1 Ori A, nebular He I 3889-Å and H8 emission (respectively the blue and red emission components) is readily seen. Since Θ^1 Ori C is much brighter than these stars, the nebular emission is relatively much fainter. We inspected the two-dimensional spectrum of Θ^1 Ori C and found weak He I and H8 emission at a level 0.5 per cent times that of the continuum. Their radial velocities were respectively 22 and 23 km s $^{-1}$ with an estimated uncertainty of 5 km s $^{-1}$. These values are in satisfactory agreement with those of O'Dell et al. (1993), who find values of 16–20 km s $^{-1}$. The velocities of the nebular H δ , H γ and H β emission lines, measured from the UCLES spectrum of Θ^1 Ori C, are all 20 km s $^{-1}$.

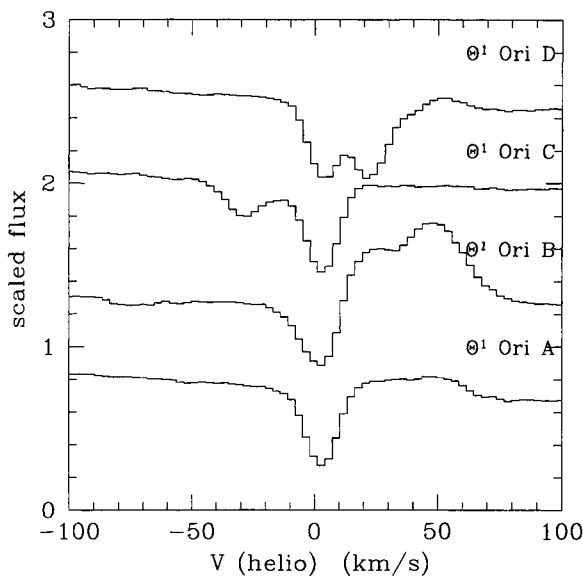


Figure 2. The non-stellar He I 3889-Å line in the Trapezium star spectra. Note the 3.5 km s^{-1} absorption component which is present in all spectra. All spectra are continuum normalized, and plotted with arbitrary offsets for clarity.

3.3 Column densities and optical depth

The equivalent widths and central velocities of the He I absorption components in the Trapezium stars were determined from the UCLES spectra and are set out in Table 2. For comparison, the measurements of the UHRF data on Θ^1 Ori C are shown as well.

In the case of Θ^1 Ori C a three-Gaussian fit through the spectrum gives the better fit to the total profile despite the fact that only two components are clearly visible in the spectrum (O'Dell et al. 1993 found this also). One may detect in Fig. 2 a very weak, higher velocity absorption component centred on a velocity of about -60 km s^{-1} in the spectrum of Θ^1 Ori C. Measurements of this feature, which contributes negligibly to the summed equivalent width (and has been left out of the sum), are included in the table with the three-component fit data and labelled as component 4.

The fifth column in Table 2 gives the column densities of helium atoms in the 2^3S state, derived using the velocity broadening ($b = 0.6 \times$ the FWHM of the line) and relevant atomic data for the transition (taken from Wiese, Smith & Glennon 1966). These calculations were performed using a curve-of-growth tool incorporated in the Starlink program package DIPSO.

To facilitate comparison with the earlier measurements by O'Dell et al. (1993, 3 km s^{-1} resolution) and Baldwin et al. (1991, 34 km s^{-1} resolution), these have been reproduced in Table 2, next to ours. The agreement in central velocities and equivalent widths is generally very good, but there are differences. First, the equivalent width of the 22 km s^{-1} velocity component in Θ^1 Ori D is measured to be twice as strong in our data as in O'Dell et al.'s data. Indeed, the spectra themselves suggest this difference. Since this feature is affected by the nebular He I emission, it is possible that the larger slit used by O'Dell et al. (2.2 arcsec, compared with our 0.9 arcsec) resulted in a stronger emission component in the extracted spectrum, thereby veiling some of the absorption line. Secondly, there is a discrepancy in the equivalent width of the absorption line of Θ^1 Ori B, with our value being much smaller. This may have to do with the manner in which the lines were measured. Since Θ^1 Ori B is the faintest of the Trapezium stars, the He I 3889-Å absorption is most affected by the neighbouring nebular emission. We decided only to measure the EW up to the

Table 2. Equivalent widths and derived column densities from the He I 3889-Å line towards Θ^1 Ori C. Errors on the equivalent width are of order 5 per cent or less.

	Our data					O'Dell et al. (1993)			Baldwin et al. (1991)	
	v_{hel} (km s $^{-1}$)	FWHM (km s $^{-1}$)	EW (mÅ)	N (10^{17} m^{-2})	v_{hel} (km s $^{-1}$)	FWHM (km s $^{-1}$)	EW (mÅ)	N (10^{17} m^{-2})	EW (mÅ)	N (10^{17} m^{-2})
Θ^1 Ori A :										
1	2.65	14.3	131.5	2.03	2.4	14.6	142.6	1.62		
Θ^1 Ori B :										
1	0.85	15.8	119.6	1.77	1.3	17.0	178.9	2.06		
Θ^1 Ori C :										
UCLES 3-component fit										
1	3.82	14.48	145.0	2.5						
2	-26.29	20.82	57.9	0.89						
total				3.4						
UHRF 2-component fit										
1										
2										
total										
UCLES 3-component fit										
1	-29.34	16.6	61.6	0.79	-30.1	16.5	59.6	0.483		
2	-9.94	22.5	33.3	0.40	-12.6	20.8	37.6	0.301		
3	3.54	14.4	128.9	1.98	2.6	13.7	130.9	1.450		
4	-60	10	(1.7)	(0.02)						
total			220.2	3.2			228.1	2.23	271 (± 41)	8
Θ^1 Ori D :										
1	3.36	13.9	123.6	1.90	2.0	13.4	127.4	1.280		
2	22.06	17.0	154.8	2.41	21.0	14.4	84.3	0.787		
total			278.4	4.3			211.7	2.07		

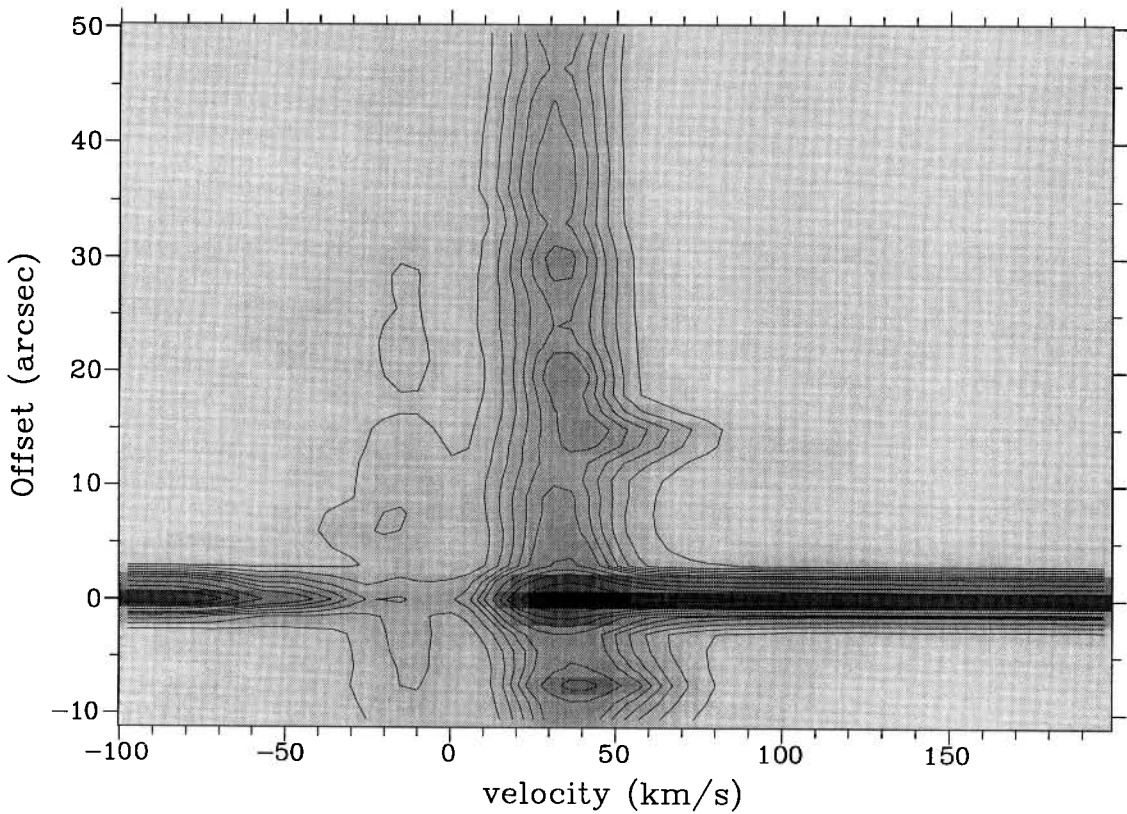


Figure 3. Contour plot of the UKIRT long-slit observations of He I 1.083 μm towards Θ^1 Ori C. The slit orientation was east–west. In the figure up is negative in RA, and thus west. The contour levels are 0.25, 0.5, 0.75, 1, 1.25, 1.5, 2, 2.5, 3 and $4 \times 10^{-11} \text{ W m}^{-2} \mu\text{m}^{-1} \text{ pixel}^{-1}$. The extracted pixel area projected on to the sky is 0.5 arcsec 2 .

continuum level, whereas O'Dell et al. have used a deblending program to separate the emission from the absorption, possibly increasing the EW of the line.

With respect to the column densities determined by O'Dell et al. (1993), there are also some discrepancies. It is not clear from their paper how O'Dell et al. derived the column densities. For example, while we might surmise that the lower column attributed by them to the $+2.6 \text{ km s}^{-1}$ component in Θ^1 Ori C is because they took it to lie on the linear part of the curve of growth, we cannot then understand why their ratio between this column and that for the -12.6 km s^{-1} component is the same as ours. In contrast, the fact that the Baldwin et al. (1991) column density is much larger than ours can be understood and can be reproduced. Since their spectral resolution was too coarse to provide a direct measurement of the line width, they adopted the turbulent velocity of 8 km s^{-1} proposed by Castañeda (1988), and used this together with their larger but less accurate equivalent width measurement. The effect of this was to treat the absorption as more saturated than higher resolution data reveal it to be.

4 THE NEAR-INFRARED PERSPECTIVE

As the He I 1.083- μm emission appears in our long-slit data as spatially extended on the sky to either side of Θ^1 Ori C, we first discuss the two-dimensional spectrum, and then go on to a description of the extracted spectrum of Θ^1 Ori C itself.

4.1 The long-slit He I 1.083- μm spectrum

Fig. 3 shows the long-slit spectrum of Θ^1 Ori C around 1.083 μm .

The strong nebular emission in the line, first discussed by Boyce & Ford (1966), is clearly visible at $v_{\text{hel}} \approx 35 \text{ km s}^{-1}$. This velocity is in excellent agreement with the higher resolution measurements of Münch (1986, 4 km s^{-1} resolution) and the results of Vaughan (1968). The origin of this emission is presumably in the principal ionization front located, in the main, behind the Trapezium. It should be noted that the reason for the velocity difference of $\approx 15 \text{ km s}^{-1}$ between this line and the H I and optical He I nebular emission, all centred at $v = 20 \text{ km s}^{-1}$ (Section 3.2; O'Dell et al. 1993), is not well understood. We return to this later.

A weaker emissive component is also present in Fig. 3, displaced about 50 km s^{-1} blueward of the main 1.083- μm emission. This component peaks at a velocity of $\approx -18 \text{ km s}^{-1}$ a few arcsec west of Θ^1 Ori C. As it fades with increasing offset from the star, the emission peak shifts to slightly less negative velocities, but never less than -10 km s^{-1} . It might be suspected that this emission should be identified with the $2^3\text{P}^0 j = 0 \rightarrow 2^3\text{S} j = 1$ 1.0829- μm minor component of the triplet transition, the strong emission at $+35 \text{ km s}^{-1}$ being due to decay from the nearly degenerate $2^3\text{P}^0 j = 1, 2$ sublevels. The primary argument against this is that the velocity separation of $\sim 50 \text{ km s}^{-1}$ is too large – it should be 34 km s^{-1} . Münch (1986) tried to overcome this problem by proposing that the stronger component is redshifted due to resonant scattering of the photons by a moving medium. His model calculations were not able to reproduce the spectra, however. It failed in particular in preventing the fainter 1.0829- μm component from being redshifted as well. Another possible means of line scattering, by moving dust particles, is ruled out because other nebular emission lines do not show a line split (e.g. H β in Fig. 7, later).

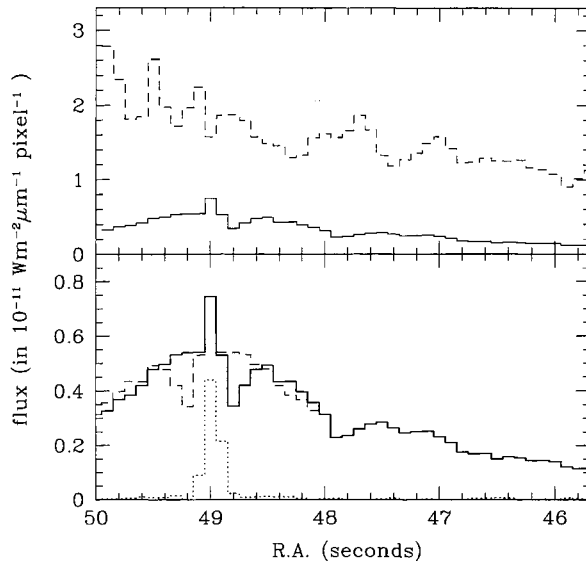


Figure 4. Upper panel: a cross-cut along the slit centred at 35 km s^{-1} on the strong background nebular $1.083\text{-}\mu\text{m}$ emission line (dashed line) and a cross-cut tracing the fainter blueshifted foreground emission at -18 km s^{-1} (solid line). Both lines are averaged over three velocity channels. The pixel area is 0.5 arcsec^2 . Lower panel: the cut across the blueshifted emission is shown on an expanded scale. To mark the position of Θ^1 Ori C a cross-cut through the stellar continuum is shown as a dotted line. The dashed line is the result of reflecting the solid line about the stellar position.

It seems more natural to associate the faint emission with the blueshifted absorption in the same wavelength range seen on-star – this absorption is unquestionably the same distinct foreground velocity component as is traced by the $3889\text{-}\text{\AA}$ line absorption. Until we return to this issue in the next section, our working hypothesis is that this weak emission component arises from the near side of M42.

An illustration of the spatial behaviour of both He I $1.083\text{-}\mu\text{m}$ emission components is provided in Fig. 4. The upper panel shows a cross-cut in the spatial direction taken at 35 km s^{-1} , along the central velocity of the background nebular $1.083\text{-}\mu\text{m}$ emission. From east to west, there is a roughly steady decline in flux. Such a trend fits in with the general trend that has been noted before for other emission lines (e.g. see Baldwin et al. 1991). This may be contrasted with the spatial dependence of the weaker blueshifted emission component at -18 km s^{-1} that is shown in the lower panel of Fig. 4: it is centred at the star (whose position is indicated by the dotted line, a cross-cut taken through the stellar continuum), and appears symmetric around the star. To emphasize this point, the dashed line drawn in the lower panel is the cross-cut reflected about the position of Θ^1 Ori C. The symmetry around the position of the star suggests that the blueshifted emission is in some manner associated with the star rather than with the background nebular radiation.

4.2 The stellar He I $1.083\text{-}\mu\text{m}$ spectrum

In Fig. 5 the extraction of a single row of the stellar spectrum at $1.083 \mu\text{m}$ is overplotted on the optical He I $3889\text{-}\text{\AA}$ absorption. The $1.083\text{-}\mu\text{m}$ absorption is deeper, dropping to 25 per cent of the continuum level, and covers a larger velocity range, with the absorption extending to blueshifted velocities of -90 km s^{-1} . On the red side, both the $3889\text{-}\text{\AA}$ and $1.083\text{-}\mu\text{m}$ absorptions set in at $\approx 18 \text{ km s}^{-1}$.

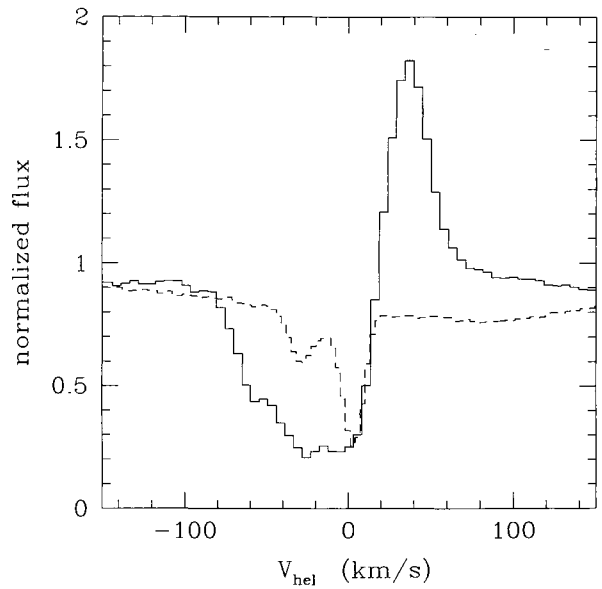


Figure 5. The He I $3889\text{-}\text{\AA}$ profile (dashed line) from the UCLES spectrum and the UKIRT $1.083\text{-}\mu\text{m}$ on-star profile (solid line). The latter spectrum is extracted from a single 1.5-arcsec pixel row and not corrected for nebular emission.

As the $3889\text{-}\text{\AA}$ and $1.083\text{-}\mu\text{m}$ absorption lines arise from the same lower state (2^3S), the optical depth in the $1.083\text{-}\mu\text{m}$ line can be calculated by multiplying the optical depth of the $3889\text{-}\text{\AA}$ line by the ratio of their respective wavelengths and oscillator strengths. This scaling is such that $\tau(1.083 \mu\text{m}) = 23.3\tau(3889\text{-}\text{\AA})$ for oscillator strengths of 0.539 and 0.0645 for the $1.083\text{-}\mu\text{m}$ and $3889\text{-}\text{\AA}$ lines respectively. From the observed depth of the $3889\text{-}\text{\AA}$ line, and the derived column densities, we find that the optical depth at the centre of the strongest component of the He I $3889\text{-}\text{\AA}$ line is about 1, implying a maximum $\tau(1.083 \mu\text{m})$ of ≈ 23 . This large optical depth would suggest that the blueshifted absorption in the line of sight towards Θ^1 Ori C should drop to zero flux after nebular subtraction.

Using the velocity parameters and column densities in Table 2 derived from the three-component fit to the $3889\text{-}\text{\AA}$ line, we have synthesized the expected blueshifted $1.083\text{-}\mu\text{m}$ absorption profile (taking proper account of all components of the triplet). Routines within the Starlink package DIPSO were used to do this. The synthetic profile, after smoothing to the instrumental resolution, is plotted in Fig. 6 and compared with a nebular-subtracted profile. The agreement is adequate. The fact that it is not perfect can be attributed to fine-scale irregularities in the extended emission that, in this case, result in its undersubtraction.

5 THE NATURE OF THE HELIUM ABSORPTION AND EMISSION

It is well established that the nebular emission lines at $v \approx 20 \text{ km s}^{-1}$ originate in the ionization front located behind the Trapezium and that the velocity component at $\sim 3 \text{ km s}^{-1}$ is present in absorption in the sight lines towards all its member stars (e.g. O'Dell et al. 1993; see also Fig. 2). The natural interpretation of the ubiquitous absorption is that a single sheet of gas moving at a mean speed of $\sim 3 \text{ km s}^{-1}$ covers the entire region. The smooth appearance of the absorption towards Θ^1 Ori C, even at a resolving power of 880 000, suggests that, in this location at least, the geometric covering factor can plausibly be approximated to unity.

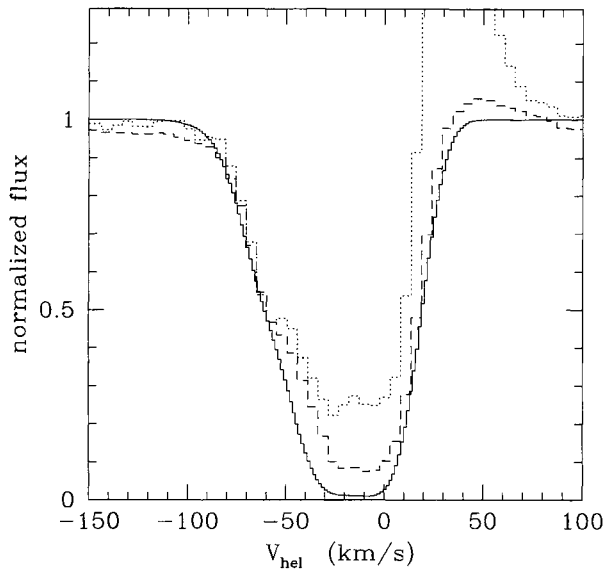


Figure 6. Synthetic spectrum of the He I 1.083- μm triplet calculated using the data listed in Table 2. The total spectrum is shown smoothed to the instrumental resolution of CGS4 (solid). In addition, the simple extraction (dotted) and a spectrum corrected for nebular emission (dashed) are shown. The latter was calculated by subtracting one pixel row of background 3 arcsec west from the central pixel row containing the spectrum of Θ^1 Ori C.

Furthermore, we have shown in the previous section that the line-of-sight optical depth at He I 1.083 μm peaks at around 23 – the run of optical depth across the line is sufficient to absorb and scatter almost all background emission in the velocity interval from -40 to $+15 \text{ km s}^{-1}$. Significantly, as will become apparent, there is an optical depth minimum of $\tau \sim 3$ at $v = -15 \text{ km s}^{-1}$.

Since the emission seen off-star at the same wavelengths as the blueshifted absorption can be shown to be optically thick, care has to be taken in deducing the process responsible for the observed emission. Can it be accounted for, straightforwardly, in terms of photoionized nebular emission? Or could the emission be starlight resonantly scattering its way through the absorbing sheet? This idea has some appeal in that it would explain why the surface brightness falls off along the slit away from Θ^1 Ori C. Or must we appeal to emission by shock-heated gas, or even a leakage of 1.0829- μm emission arising in the background nebula through the foreground sheet? We consider these possibilities in turn, beginning in the next section with an examination of the nebular emission hypothesis.

5.1 A limit on the electron density from Br γ

Before a calculation can be made of the emission to be expected in the case of a conventional photoionized ($\sim 10\,000 \text{ K}$) nebula, it is necessary to make an assessment of the prevailing electron density. We can place an upper limit on this quantity for the foreground clouds by first predicting the Br γ flux at the velocities of the blueshifted He I 3889- \AA absorption lines, and then comparing it with the results of our Br γ observation. The details of this procedure and the results obtained are given in Appendix A.

The off-star Br γ spectrum is shown in Fig. 7. The strong nebular component at $25 \pm 5 \text{ km s}^{-1}$ is readily visible, but there appears a blueshifted emission feature at -50 km s^{-1} rather than at the expected -18 km s^{-1} . It seems unlikely, however, that this weak emission feature is associated with the Br γ line itself since we do

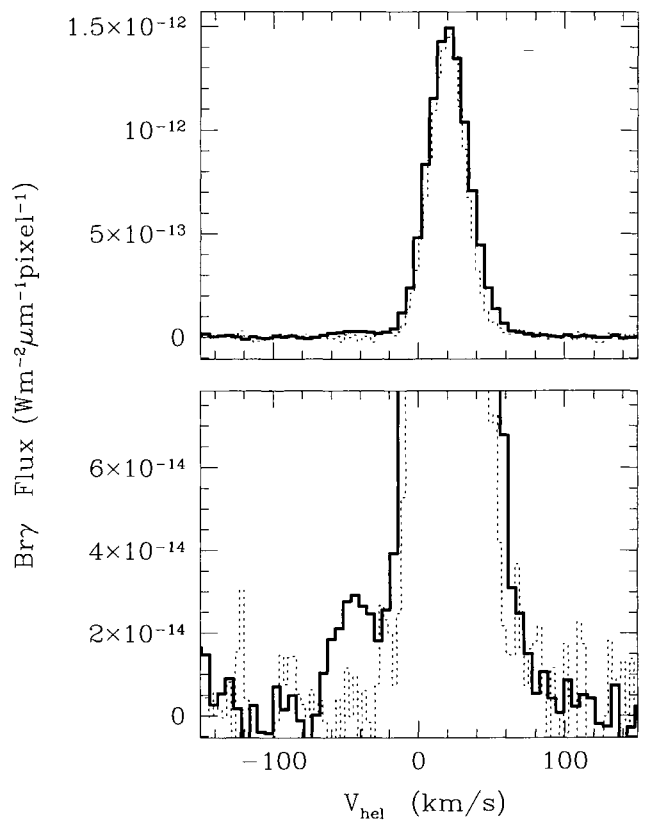


Figure 7. Upper panel: overplot of nebular Br γ (thick, solid line) and H β emission (dashed line). The H β emission has been scaled to match the Br γ emission and the Br γ line has been shifted -5 km s^{-1} to match the peaks. The flux level has been corrected for interstellar reddening (Section 2). Lower panel: same as above, but with the vertical scale expanded. The feature at -50 km s^{-1} is not present in H β .

not detect an analogous feature on the short-wavelength side of the H β nebular profile, observed 16 d earlier (see Fig. 7). Lacking a satisfactory alternate identification for it, we suspect the feature is a ‘ghost’ of the main Br γ emission due to the interference that is also responsible for the fringing affecting this wavelength setting. Comparisons with data on other strong emission-line objects, observed during the same night at the same wavelength, indicate that a similar velocity component is present in those spectra as well.

We must settle, therefore, for an upper limit on the blueshifted Br γ emission and hence on the electron density. The rms noise in the Br γ spectrum is $\approx 4 \times 10^{-15} \text{ W m}^{-2} \mu\text{m}^{-1} \text{ pixel}^{-1}$. If the component had a total width of nine velocity channels (as does the He I 1.083- μm line emission), and a constant flux matching the 2σ level, its integrated flux would be $1.3 \times 10^{-18} \text{ W m}^{-2} \text{ pixel}^{-1}$ or $2.6 \times 10^{-18} \text{ W m}^{-2} \text{ arcsec}^{-2}$ (the ‘pixel’ in this case is the extraction pixel of $0.33 \times 1.5 \text{ arcsec}^2$). A higher upper limit on the undetected Br γ flux could be allowed if this component were broader than the He I 1.083- μm line, as might be the case if thermal broadening dominates the line width (see Section 3.1). The upper limit on the observed blueshifted Br γ surface brightness is thus $\sim 2.5 \times 10^{-18} \text{ W m}^{-2} \text{ arcsec}^{-2}$. After dereddening, this is comparable with the surface brightness deduced in Appendix A for a density of 10^{10} m^{-3} ($5 \times 10^{-18} \text{ W m}^{-2} \text{ arcsec}^2$). The electron density could, in fact, be well below this limit since one of the assumptions in our chain of reasoning is that the H II region extends no further than the He II region, which may not be the case. A relevant comparison is that the

Table 3. The He I 1.083- μm C/R ratio as a function of electron density and temperature, calculated according to the prescription of Clegg (1987).

T (K)	n_e (m^{-3})	10^9	10^{10}	10^{11}
10 000		2.0	6.2	7.8
20 000		4.9	12.9	14.2

electron density quoted as typical of the background nebula by Baldwin et al. (1991) is in fact 10^{10} m^{-3} , the same as our upper limit. A deeper observation of the Br γ line than presently available is desirable.

5.2 A limit on the contribution to the blueshifted He I 1.083- μm emission from photoionized gas

Armed with an upper limit on the electron density, we can now set an upper limit on the emission that could arise from collisional excitation and recombination in the foreground cloud. If this region is heated just by photoionization, a kinetic temperature within a thousand degrees or so of 10^4 K is likely.

Before embarking on this, it is important to realize that the visibility of photons created internally by collisions or recombinations is not in fact limited by the non-negligible optical depth of the medium. This is because the destruction probability of He I 1.083- μm photons formed in, or travelling into, the medium is very small. In other words, the medium is effectively optically thin (see Appendix B).

Let us now determine the surface brightness generated by recombination into and collisional excitation of the He I 1.083- μm line. For an electron density of 10^{10} m^{-3} and $T = 10^4 \text{ K}$, we have $N_{2^3S}/N_{\text{He}^+} = 4.3 \times 10^{-6}$ (from equation A1). The column in He $^+$ is thus about $7.0 \times 10^{22} \text{ m}^{-2}$, for $N_{2^3S} = 3 \times 10^{17} \text{ m}^{-2}$. This can be turned into a recombination line yield and corrected to account for collisions by multiplying by the factor $(C/R + 1)$. C/R is the ratio between the contributions of collisional excitation from 2^3S and He $^+$ recombination to the population of the 2^3P^0 upper level. Following the prescription of Clegg (1987) we obtain the results set out in Table 3. From this it can be seen that C/R is ~ 7 for $n_e \gtrsim 10^{10} \text{ m}^{-3}$ at 10 000 K. The surface brightness in the He I 1.083- μm line contributed by recombination alone in these conditions can be calculated using the emissivities tabulated in Osterbrock (1989) – it is $2.2 \times 10^{-17} \text{ W m}^{-2} \text{ arcsec}^{-2}$. On multiplying by $(C/R + 1)$ this converts to a total upper limit on the surface brightness of $1.8 \times 10^{-16} \text{ W m}^{-2} \text{ arcsec}^{-2}$. If we had chosen a temperature of 20 000 K, this figure would roughly double, mainly in response to the increase in C/R .

The observed surface brightness just off-star is $8 \times 10^{-16} \text{ W m}^{-2} \text{ arcsec}^{-2}$. Since this is actually $1.5 \times 10^{-15} \text{ W m}^{-2} \text{ arcsec}^{-2}$ after dereddening, the flux that is ‘predicted’ for $T = 10 000 \text{ K}$ and $n_e = 10^{10} \text{ m}^{-3}$ is only of order 10–20 per cent of the observed flux. Furthermore, if one considers that the electron density could well be significantly lower than that adopted in this calculation, it is clear that the observed blueshifted emission cannot be attributed straightforwardly to photoionized gas presenting the column deduced from the observed 3889- \AA absorption.

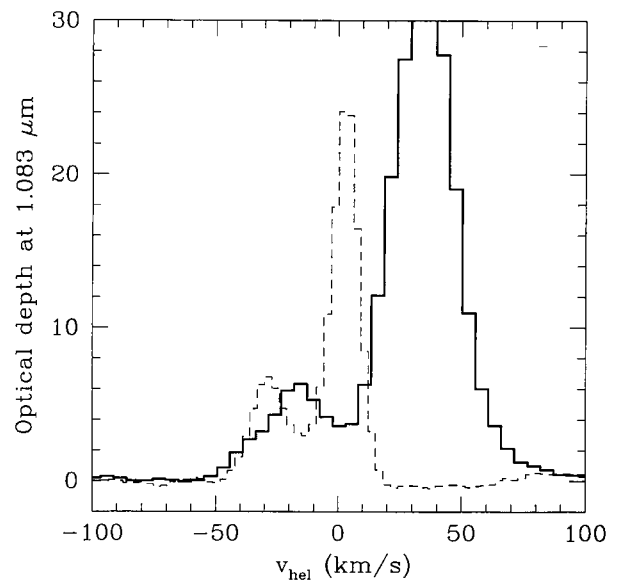


Figure 8. The optical depth in the 1.083- μm line (dashed), based on τ_{3889} which was calculated from the depression of the continuum of the 3889- \AA line. To obtain $\tau_{1.083}$, this is multiplied by 23 (see text). The solid line is the He I 1.083- μm off-star emission on an arbitrary scale. It is apparent that the maximum of the emission is present at the velocities where the minimum optical depth occurs.

5.3 Evidence for the blueshifted He I 1.083- μm line emission as light leaking through the foreground sheet

If the same ionized column as is responsible for the observed blueshifted 3889- \AA absorption cannot be the source of the off-star emission at the same velocity, the only likely alternative is that the emission arises from another body of gas lying *behind* the optically identified absorbing sheet. Evidence that points in this direction is shown in Fig. 8. In it the velocity profile of the off-star emission as observed close to the star is superposed on the run of optical depth with velocity, deducible directly from the 3889- \AA absorption profile. It is striking that the off-star emission ‘seeps through’ at just those velocities where the optical depth reaches a minimum. The same impression can be gained from the results of Münch’s (1986) higher spectral resolution ($R = 75 000$) observations of the He I 1.083- μm line obtained through a circular aperture at a number of pointings within the nebula. Münch’s data eliminate the possibility that our detected off-star emission might be an unresolved blend of two weak emission features centred at the same velocities as the prominent absorption components in the 3889- \AA line.

If the emission arises in some region behind the absorbing sheet, the first possibility to consider is that it may simply be the illuminating starlight that resonantly scatters its way through the sheet (remembering that the destruction probability, ϵ , associated with the He I 1.083- μm line is probably very small, see Appendix B). This idea can be shown to be unworkable on basic energetic grounds. We find that the total flux entering the long-slit spectrum over 51 pixels is $\sim 1.7 \times 10^{-14} \text{ W m}^{-2}$. Of course the total flux of the line emission is very likely to be much larger, as we only observe a strip on the sky of width 1 arcsec. If the emission is circularly symmetric, the total line flux is around 50 times larger, or $\sim 8 \times 10^{-13} \text{ W m}^{-2}$. On dividing this number by the observed continuum flux from the star ($7.5 \times 10^{-11} \text{ W m}^{-2} \mu\text{m}^{-1}$), one may arrive at the continuum bandwidth needed to match the integrated

off-star flux. We find this to be $\sim 3000 \text{ km s}^{-1}$, a width that is far in excess of the observed line width. The situation is in fact worse than this because the resonantly scattered light emerging from the near side of the sheet can, in any case, only be of order $1/\tau$ the brightness of that which was incident on the far side (see Mihalas 1978).

A further possibility to consider is that there may be a shock-excited source of He I 1.083- μm emission. This has the attraction of providing a ready explanation for the apparent centring of emission along the slit on Θ^1 Ori C as illustrated in Fig. 4. Although the spatial coverage around Θ^1 Ori C is limited to ~ 15 arcsec east and ~ 45 arcsec west, the figure indicates a symmetrical distribution of the blueshifted emission centred on the star, while the background nebular emission component shows a shallow steady gradient. The impression given is that the two components are uncorrelated. The spatial symmetry with respect to Θ^1 Ori C, and the lack of correlation with the background nebula, leaves as the most viable option a connection with the star itself as energy source.

As do all O stars of similar spectral type, Θ^1 Ori C powers a high-momentum wind. Recent *Hubble Space Telescope* images of the region around the Trapezium demonstrate very graphically the dynamical impact of this wind on condensations within its grasp (Johnstone *et al.* 1996). A possibility to consider, therefore, is that the extended blueshifted emission betrays a faint but widespread shock front, arising from snow-ploughing of the fast wind from Θ^1 Ori C into the circumstellar medium.

Given the metastable character of the He I 2^3S state, we can expect that the blueshifted He I 1.083- μm emission must have its counterpart in absorption along the line of sight towards Θ^1 Ori C. This is not a problem as long as its contribution to the total absorbing column is modest so that we might still observe the effect of the emission ‘leaking through’ the overlying He I 2^3S column. For example, it would have little impact on our earlier calculation of the photoionized emission from the foreground absorber (Section 5.2) if around 10 per cent of the total column were linked to the blueshifted emission. Can such a small column of gas produce as much He I 1.083- μm emission as is required of it here? Based on considerations such as those rehearsed in Section 5.2, a substantially increased gas temperature alone could not suffice – an electron density of 10^{11} m^{-3} or more is probably required as well (a figure to be compared with our upper limit on the foreground absorber electron density of $\sim 10^{10} \text{ m}^{-3}$).

In principle, a test of this concept would be to look for evidence of emission at similar velocities and locations to those giving rise to the blueshifted emission in other more easily analysed spectral lines. In the case of Br γ this is hampered by the apparent presence of a ‘ghost’ in the line profile. Preliminary attempts to predict the Br γ line profile from the He I 1.083- μm profile using simple nebular theory may indicate that the observed Br γ emission at the relevant velocities is too small, but given the free parameters at our disposal, and the uncertainty in the observation, we can not be confident of this as yet. Other emission lines such as, for example, the much-exploited density-sensitive [S II] lines at 6716 and 6731 Å are unfortunately unlikely to be useful in this case because of the relatively high density anticipated for the emitting gas. Better alternatives might be found in the spectra of doubly or triply ionized iron.

5.4 On the possibility of leaking background nebular emission

If there is significant 1.0829- μm emission from the background nebula, can it be leaking through the opaque foreground sheet? If, as seems plausible, the background nebula is optically thick in the He I

1.083- μm line, the flux ratio between the 1.0829- and 1.0830- μm components need not be as extreme as the optically thin value of 1:8. This uncertainty in the flux ratio, together with the impossibility of reconstructing from the data the blueshifted emission incident on the far side of the foreground absorbing sheet, makes a quantitative assessment of this idea unfeasible. Indeed, there are similar difficulties in reconstructing the background 1.0830- μm emission. The anomalously high mean velocity of this component ($\sim +35 \text{ km s}^{-1}$, as opposed to $\sim +20 \text{ km s}^{-1}$ for other transitions) could, in part, be due to the high opacity of the foreground sheet eating into its blue wing (see Fig. 6 – but note that the synthetic absorption profile in this case has already been smoothed with the instrumental profile). Furthermore, we have no information that would allow us to determine if absorption due to intervening material behind Θ^1 Ori C is a significant factor. The example of the 22 km s^{-1} absorption component in the spectrum of Θ^1 Ori D (Fig. 2) which may originate between Θ^1 Ori C and the background nebula (as suggested by O’Dell *et al.* 1993) illustrates that this could well be an issue.

We conclude that this model for the blueshifted emission cannot be ruled out but that it remains unsatisfactory in that it does not simply explain why the blueshifted emission should depart from the trend apparent in the stronger redshifted component and decline away from the position of Θ^1 Ori C.

6 CONCLUSIONS

We have investigated the neutral helium absorption and emission system towards the exciting star of the Trapezium, Θ^1 Ori C. Our conclusions can be summarized as follows.

(i) The He I 3889-Å blueshifted absorption system traces the same material as the He I 1.083- μm absorption. Even at a spectral resolution of almost one million, the 3889-Å absorption profile is very smooth, suggesting a simple broadening mechanism and homogeneity. The combination of the He I column density deduced from the 3889-Å line with the non-detection of Br γ emission at the same velocities sets an upper limit on the electron density in this medium of 10^{10} m^{-3} .

(ii) The blueshifted He I 1.083- μm emission component detected off-star at the same velocities as the on-star absorption is most plausibly explained as emission leaking through the layer of gas responsible for most, if not all, of the absorption. The spatial distribution of the emission hints at a physical connection with Θ^1 Ori C and does not follow that of the brighter emission component associated with the background nebula. This encourages us to surmise that the blueshifted emission arises in a large-scale shock front, provoked in some way by the wind of Θ^1 Ori C.

We briefly return to the significance of the absorbing gas traced so clearly by the 3889-Å blueshifted absorption profile. Because we have had to argue that the gas emitting at the same velocities in the He I 1.083- μm line is probably behind this foreground entity, the existence of the emission does not help at all in understanding the dynamical origin of the absorption. It remains an intriguing fact that there are apparently three velocity components involved along the sight line to Θ^1 Ori C (at ~ 0 , -30 and, now, -60 km s^{-1} in round numbers) and that only the most redshifted of them is of sufficient lateral extent to be seen in the sight lines towards the other Trapezium stars. For this component, we now have an upper limit on the electron density that allows us to estimate a minimum physical depth of around $4 \times 10^{13} \text{ m}$ or ~ 200 au.

We end with the note that our study suggests that the He I 1.083- μm line may, on occasion, sensitively probe subtle dynamical effects involving modest columns of gas denser than those traced by the commonly exploited optical forbidden lines (e.g. the [O II] and [S II] lines that are density sensitive up to $n_e \sim 10^{10} \text{ m}^{-3}$). Since He I 1.083 μm is not a forbidden transition, and yet is readily collisionally excited, its emissivity continues to increase as the square of the electron density above $n_e \sim 10^{10} \text{ m}^{-3}$, without a strong dependence on temperature at temperatures typical of ionized nebulae.

ACKNOWLEDGMENTS

The allocation of time on UKIRT and the Anglo-Australian Telescope was awarded by PATT, the United Kingdom allocation panel. This work was entirely funded by the Particle Physics and Astronomy Research Council of the United Kingdom.

REFERENCES

- Adams W. S., 1944, PASP, 56, 119
 Baldwin J. A., Ferland G. J., Martin P. G., Corbin M. R., Cota S. A., Peterson B. M., Slettebak A., 1991, ApJ, 374, 580
 Baldwin J. A. et al., 1996, ApJ, 468, L115
 Boyce P. B., Ford W. K., 1966, PASP, 78, 163
 Cardelli J. A., Clayton G. C., Mathis J. S., 1989, ApJ, 345, 245
 Castañeda H. O., 1988, ApJS, 67, 93
 Clegg R. E. S., 1987, MNRAS, 229, 31p
 Drew J. E., Bunn J. C., Hoare M. G., 1993, MNRAS, 262, 19
 Howarth I. D., Prinja R. K., 1989, ApJS, 69, 527
 Johnstone D. et al., 1996, BAAS, 189, 49.12
 Koornneef J., 1983, A&A, 128, 84
 Mihalas D., 1978, Stellar Atmospheres. Freeman, San Francisco, p. 312
 Münch G., 1986, Mitt. Astron. Ges., 63, 65
 Murdoch K. A., Drew J. E., 1994, in Thé P. S., Pérez M. R., van den Heuvel E. P. J., eds, ASP Conf. Ser. 62, The Nature and Evolutionary Status of Herbig Ae/Be Stars. Astron. Soc. Pac., San Francisco, p. 377
 O'Dell C. R., Valk J. H., Wen Z., Meyer D. M., 1993, ApJ, 403, 678
 Osterbrock D. E., 1989, Astrophysics of Gaseous Nebulae and Active Galactic Nuclei. University Science Books, Mill Valley, CA
 Peimbert M., 1967, ApJ, 150, 825
 Peimbert M., Luridiana V., Torres-Peimbert S., 1995, Rev. Mex. Astron. Astrofis., 31, 147
 Rieke G. H., Lebofsky M. J., 1985, ApJ, 288, 618
 Savage B. D., Jenkins E. B., 1972, ApJ, 172, 491
 Stahl O. et al., 1996, A&A, 312, 539
 Storey P. J., Hummer D. G., 1995, MNRAS, 272, 41
 Straizys V., Kurliene G., 1981, Ap&SS, 80, 353
 van der Werf P. P., Goss W. M., 1989, A&A, 224, 209
 Vaughan A. E., 1968, ApJ, 154, 87
 Walborn N. R., 1981, ApJ, 243, L37
 Walborn N. R., Nichols J. S., 1994, ApJ, 425, L29
 Wiese W. L., Smith M. W., Glennon B. M., 1966, Atomic Transition Probabilities, Vol. II, Hydrogen through Neon. Natl. Stand. Ref. Data Ser. 20

APPENDIX A: ESTIMATION OF THE ELECTRON DENSITY FROM THE Br γ SURFACE BRIGHTNESS

The column density of the 2³S level, N_{2^3S} , which was derived from the He I 3889- \AA absorption-line measurements, can be transformed into a column density of He $^+$, N_{He^+} , using the relation presented by Peimbert, Luridiana & Torres-Peimbert

(1995; see also Clegg 1987):

$$\frac{N_{2^3S}}{N_{\text{He}^+}} = \frac{5.62 \times 10^{-6} t_4^{-1.19}}{1 + 3130 t_4^{-0.5} n_e^{-1}} = g(n_e, T), \quad (\text{A1})$$

with t_4 the electron temperature in 10⁴ K and n_e the electron density in cm⁻³.

Since the size of the region where helium is fully ionized is smaller than or equal to that of the H II region, we can use this relation to derive a minimum value for the N_{He^+} column density. In turn, this quantity can be used in Case B recombination theory to 'predict' the (minimum) optically thin Br γ flux. As it has been shown that most H I recombination lines emitted by the much brighter background nebula are optically thin (Baldwin et al. 1991), it is a safe assumption that any foreground emission will be optically thin also. We can therefore write the Br γ line surface brightness as

$$j_{\text{Br}\gamma} = \frac{1}{4\pi} N_{\text{H}^+} n_e \alpha_{\text{Br}\gamma}^{\text{eff}} \frac{hc}{\lambda} \quad \text{W m}^{-2} \text{ sr}^{-1}, \quad (\text{A2})$$

where N_{H^+} is the column density of ionized hydrogen and $\alpha_{\text{Br}\gamma}^{\text{eff}}$ the effective recombination coefficient. If the abundance of helium with respect to hydrogen by number is 0.088 (Baldwin et al. 1991), we have a lower limit on the column density of ionized hydrogen of

$$N_{\text{H}^+} \geq \frac{N_{2^3S}}{g(n_e, T) 0.088}. \quad (\text{A3})$$

On combining this with the expression for the line surface brightness, we obtain

$$j_{\text{Br}\gamma} \geq 0.904 \frac{N_{2^3S}}{g(n_e, T)} n_e \alpha_{\text{Br}\gamma}^{\text{eff}} \frac{hc}{\lambda}, \quad (\text{A4})$$

where the product $\alpha_{\text{Br}\gamma}^{\text{eff}} \frac{hc}{\lambda}$ is an emissivity that may be calculated in Case B using the routine of Storey & Hummer (1995). At a temperature of 9000 K, this product is $3.84 \times 10^{-40} \text{ W m}^3$ (dropping to $1.86 \times 10^{-40} \text{ W m}^3$ at 17 000 K). Over the density range 10^9 – 10^{11} m⁻³, its value changes only in the last decimal place.

The surface brightness in Br γ calculated according to equation (A4) is only weakly sensitive to the adopted temperature in the domain of interest ($T \geq 10^4$ K). For example, doubling the assumed temperature causes the derived surface brightness to change by no more than a few per cent. The primary dependence of the expression as a whole is indeed on the assumed electron density. The (minimum) Br γ surface brightness (in units of $N_{17} \text{ W m}^{-2} \text{ arcsec}^{-2}$, where N_{17} is the neutral helium 2³S column density in 10^{17} m^{-2}) is 0.55×10^{-18} , 1.7×10^{-18} , and 13×10^{-18} at electron densities of 10^9 , 10^{10} and 10^{11} m⁻³ respectively.

From the He I 3889- \AA absorption we determined the 2³S column density to be $\sim 3 \times 10^{17} \text{ m}^{-2}$. The expected unreddened surface brightness is thus about $5 \times 10^{-18} \text{ W m}^{-2} \text{ arcsec}^{-2}$ for $n_e = 10^{10} \text{ m}^{-3}$. The approximate correction for reddening is to halve this figure (see Section 2.3). In principle, a comparison can now be made with the observed blueshifted Br γ emission.

APPENDIX B: ON THE EFFECTIVE OPTICAL DEPTH OF THE FOREGROUND SHEET TO THE He I 1.083- μm LINE

The destruction probability ϵ for an equivalent two-level atom may be expressed as

$$\epsilon = \frac{C_{21}}{C_{21} + A_{21}(1 - e^{hv/kT})^{-1}}, \quad (\text{B1})$$

where A_{21} is the Einstein emission coefficient ($1.022 \times 10^7 \text{ s}^{-1}$ for the He I 1.083- μm transition), and C_{21} is the collisional de-excitation rate ($= n_e q_{21}$, with $q_{21} = 0.247 \text{ m}^{-3} \text{ s}^{-1}$ at 10^4 K). This quantity is the fraction of helium atoms in the 2^3P^0 state that are collisionally de-excited to the 2^3S level (transitions via other levels are ignored in this approximation). For an electron density of $\sim 10^{10} \text{ m}^{-3}$, the destruction probability is only of order 10^{-10} . The product $\epsilon\tau$, where τ is the optical depth in the line, can then be thought of as the probability that a line photon will be destroyed during its passage through the medium. Since τ is never greater than

~ 23 at any wavelength in the profile, this product is very small, suggesting that the medium may be regarded as effectively optically thin. This carries the sense that practically all photons created within it will scatter their way out. Furthermore, as long as the medium is reasonably uniform, with photon creation efficiency and opacity being similar functions of position, the far face and the near face of the medium will be equally bright.

This paper has been typeset from a $\text{T}_E\text{X}/\text{L}^A\text{T}_E\text{X}$ file prepared by the author.